Biomass and Bioenergy 131 (2019) 105402

Contents lists available at ScienceDirect

Biomass and Bioenergy

journal homepage: http://www.elsevier.com/locate/biombioe

Research paper

Predicting and analyzing the performance of biomass-burning natural draft rocket cookstoves using computational fluid dynamics

Anamol Pundle [a], Benjamin Sullivan [a], Paul Means [b], Jonathan D. Posner [a,c,d], John C. Kramlich [a,*]

[a] Department of Mechanical Engineering, University of Washington, Seattle, WA, 98195, USA
[b] BURN Design Labs, Vashon, WA, 98070, USA
[c] Department of Chemical Engineering, University of Washington, Seattle, WA, 98195, USA
[d] Department of Family Medicine, University of Washington, Seattle, WA, 98195, USA

ARTICLE INFO

Keywords:
Cookstove
CFD
Combustion
Energy efficiency
Biomass

ABSTRACT

Nearly three billion people in the world today rely on biomass for their cooking needs. Indoor cooking using biomass has been identified as a major cause of respiratory illnesses, resulting in four million premature deaths every year. Improved biomass cookstoves may help mitigate this challenge. This paper presents a two-dimensional axisymmetric steady-state computational fluid dynamics (CFD) model of a biomass burning, natural draft rocket cookstove. The CFD model includes coupled sub-models representing combustion, turbulence, and heat transfer. The model is validated against experimental data and used to predict temperatures and flow inside the cookstove, including the airflow rate through the cookstove and heat transfer to the cookpot. We find that the excess air is typically many times stoichiometric air during standard operating conditions and is sensitive to flow field obstructions. We analyze the effects of geometric and operational features such as the pot support height, secondary air entrainment, cone-deck shape, and baffle placement within the cookstove on the flow, airflow rate, mixing, and stove thermal efficiency. The model shows that secondary air entrainment, though ineffective by itself, increases turbulent mixing when used in conjunction with a central baffle but reduces thermal efficiencies due to enhanced heat transfer to the walls. We find that a lower pot support height decreases the airflow rate and increases thermal efficiency. We model thirty-six cone-deck configurations and find that the cone-deck shape primarily affects the airflow rate through the stove, with more constricted designs leading to higher thermal efficiencies.

1. Introduction

Nearly three billion people, largely in regions of Africa and Southeast Asia, depend on biomass for their cooking needs [1]. Cooking with biomass produces particulate matter, which has been identified as a significant contributor to cancer, respiratory diseases, and cardiovascular ailments. Women and children are disproportionally affected because the vast majority of cooking in developing countries is performed by women in the presence of their children [2]. Indoor air pollution has been estimated to contribute to over 4 million premature deaths every year [3], much of which is attributed to biomass combustion. Biomass combustion also contributes to climate change through the emission of greenhouse gases and black carbon, which is considered to be the second most important contributing species to climate change after CO_2. About 25% of the worldwide black carbon emission is due to biomass combustion [4]. Gathering wood for fuel contributes to deforestation, and the scarcity of wood fuel is a growing problem in several developing countries [5].

The health and environmental impacts of cooking with rudimentary biomass stoves drive the need to develop low emission, high efficiency improved cookstoves. A commonly used improvement is a natural draft, biomass burning cookstove called a 'rocket' stove. These stoves typically consist of a cylindrical shell that encloses the fire, with the combustion gas being directed towards the cookpot that sits atop the cylinder. The fuel is introduced through an opening in the side of the combustion chamber. The performance of these cookstoves is usually established through testing guidelines developed by the International Standards Organization (ISO). The ISO 19867–1:2018 guidelines provide a 4-tier

* Corresponding author.
E-mail address: kramlich@uw.edu (J.C. Kramlich).

https://doi.org/10.1016/j.biombioe.2019.105402
Received 19 February 2019; Received in revised form 30 August 2019; Accepted 10 October 2019
Available online 20 November 2019

system for cookstove performance (1 being the lowest level of performance and 4 being the highest), measured using the Water Boiling Test protocol [6]. Performance parameters measured include fuel use (thermal efficiency), emissions (CO, $PM_{2.5}$) and indoor emissions (CO, $PM_{2.5}$). Jetter et al. [7] examined the laboratory performance of 22 different cookstoves and a three stone fire burning six kinds of fuel. Several rocket stoves showed significant improvements in thermal efficiency, combustion efficiency and pollutant emissions over the three stone fire; however, improvements still need to be made to natural draft stoves' $PM_{2.5}$ emissions and thermal efficiency to meet the WHO recommended guidelines. The problem is exacerbated by the fact that field performance is generally much worse than lab performance. Roden et al. [8] found that, on average, PM emission factors measured in the field were over three times larger than laboratory measured PM emission factors for the same cookstove. In a 2007 study, Smith el al. [9]investigated three sites where improved cookstoves were introduced, and found that the site with the lowest ambient $PM_{2.5}$ concentration exceeded WHO guidelines by a factor of ten.

Stoves are often designed using an iterative process, i.e., building a prototype, testing it, then refining stove parameters until an acceptable design is found [10]. This process is resource intensive, time consuming, and does not provide insight into the physics governing the performance of the cookstove. Computational modeling can serve as a complement to iterative design in order to reduce time and resources required to meet the target goals of a particular stove. Numerical models can also provide details about physical processes inside the cookstove, the knowledge of which can be used by stove designers to design better performing cookstoves. The effect of geometric parameters on combustion and mixing may also be studied without undergoing the expensive and time-consuming process of building and testing cookstoves.

There are few reported studies on the numerical simulation of cookstoves. As pointed out by MacCarty and Bryden in their review of cookstove modeling, of the five hundred journal articles published on cookstove development in the last thirty years, fewer than thirty have focused on modeling [11]. Early modeling work was conducted by Baldwin [12] who developed a steady-state heat transfer model to study the effect of the length and width of the channel between the cookpot and pot skirt on the heat transferred to the cookpot. The model predicted that a smaller channel gap and longer channel length increased the heat transfer to the pot, but this was not experimentally validated. The model made several unrealistic assumptions, and the author cautioned against its use as a predictive tool. Agenbroad et al. [13,14] developed a Bernoulli equation-based model with a constant loss coefficient to predict the flow rate through a rocket elbow without a pot, given the geometry of the elbow and the firepower. The model was validated with excess air and temperature measurements for a range of firepowers. The model results were sensitive to the loss coefficient, which was used as a model tuning parameter. Shah and Date [15] developed a simplified four-zone coupled thermochemical model to predict the thermal efficiency, composition of combustion products, and excess-air factors for an experimental stove. The effect of cookstove geometry, fuel characteristics and other ambient conditions were investigated.

CFD based models of cookstoves have also been developed [11, 16–19]. CFD models are more computationally demanding than analytical ones, but are capable of handling complex geometries, require fewer assumptions, and can provide detailed information about heat transfer, mixing and combustion processes within the cookstove. Burnham-Slipper [16] developed a two dimensional axisymmetric steady state RANS model coupled with a pyrolysis sub-model, including combustion in the gas phase modeled by a single step reaction. The model considered the simple geometry of a cylinder as the riser with an aluminum plate on top to simulate the cooking surface. Heat transfer was modeled, though radiation due to soot was neglected. The model was compared to temperature and heat transfer data from experiments. The model predicted burn rates and temperatures inside the stove accurately for some cases but not for others. Miller-Lionberg [17] developed a three dimensional LES model with combustion modeled by a mixture fraction method and soot predicted by the Moss-Brookes model, along with heat transfer to the environment. Inputs to the model were the geometry of an improved rocket stove and fuel flow rates at low and high firepower. The model predicted the overall heat transfer to the pot accurately for high firepower, but the low firepower case had an error of 29%. CO and PM emissions were under-predicted by four and ten orders of magnitude, respectively. Wohlgemuth et al. [18] studied the effect of the gap between the pot and pot skirt using a axisymmetric RANS CFD model. The study suggested that there is an optimum distance between the pot and pot skirt that maximizes thermal efficiency, which can be increased further by insulating the pot skirt.

While these models have advanced the state of the art, they have largely been validated and used for a limited number of geometries, often without considering actual stove design features. Combustion has either not been modeled, or modeled with very simple chemical kinetic mechanisms (sometimes with just a single step reaction). Heat transfer is often modeled without considering the presence of soot, which significantly affects the temperature distribution and heat transfer from the cookstove. The influence of design features, such as custom shaping of the cone deck, secondary air entrainment ports, and baffles on the stove performance has not been studied. The underlying physics behind why certain configurations result in better emissions and thermal efficiencies has not been fully explained.

In this work, we develop a steady-state, two-dimensional axisymmetric CFD model to simulate the fluid flow, combustion, turbulence and heat transfer in a wood burning, natural draft rocket stove. The goal of the model is to provide a link between (1) stove design features, (2) stove physics (flow, heat transfer, chemistry), and (3) stove thermal performance. The design features include geometric parameters such as the pot support height, cone-deck shape, secondary air entrainment and the insertion of baffles. Through this process we gain an understanding of the physics at work inside the cookstove, which can be used by stove designers to alter the flow field and temperature distribution inside the cookstove in order to enhance heat transfer to the pot and reduce emissions by increasing turbulence and mixing.

2. Computational model

2.1. Model geometry

The computational domain is a simplified representation of a side-fed natural draft rocket stove, a schematic of which is shown in Fig. 1. Air enters from the primary air inlet at the bottom of the stove and wood volatiles are discharged uniformly from three toroidal fuel inlets. The toroidal fuel inlets have approximately the same surface area as the nominal four sticks of wood used in the experimental work. The wood volatiles and air mix in the combustion chamber, which is a cylindrical cavity of 100 mm diameter and 291 mm height, giving rise to flaming combustion. The riser provides a flow path above the combustion chamber. Secondary air is entrained into the riser 150 mm above the primary air inlet. The hot combustion gases flow towards the 280 mm diameter pot that is placed above the riser atop a conical-shaped cone deck. The cone deck serves as a gradual area expansion for the gas flow, to prevent flow separation, and directs flow over the bottom of the pot and out to the 340 mm diameter pot skirt. A pot skirt is an optional stove feature that directs hot combustion gases along the sides of the pot and improves heat transfer to the pot [18].

2.2. Mathematical model

We solve the Reynolds-averaged conservation equations of mass, momentum, energy, and species transport. We model turbulence using the Realizable $k-\varepsilon$ turbulence model, which is a modified form of the standard two-equation $k-\varepsilon$ model [20]. Transport equations for turbulent kinetic energy, k, and the turbulent dissipation rate, ε [21] are

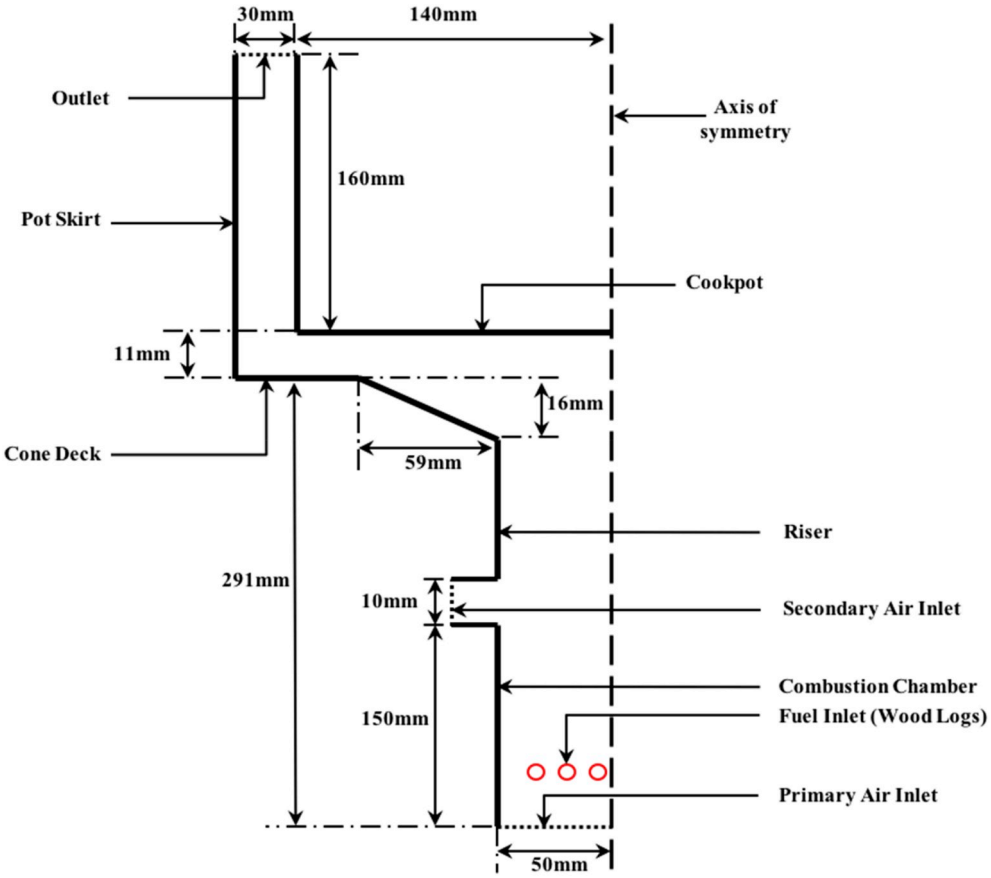

Fig. 1. Schematic of axisymmetric computational model. Air enters from the primary and secondary air inlets; fuel enters from the circular-shaped fuel inlet. The flow exits at the outlet.

solved. We close the momentum equation by calculating the turbulent eddy viscosity,

$$\mu_T = \rho C_\mu \frac{k^2}{\varepsilon} \tag{1}$$

from the turbulent kinetic energy k, the turbulent dissipation rate ε, the density ρ, and C_μ, a model parameter that is a function of the strain rate tensor, k, and ε [20]. We model radiation by solving the radiative transfer equation (RTE) by the discrete ordinates method, using the S_4 approximation [22]. While the presence of soot is important for heat transfer by radiation, we do not explicitly model the soot, instead opting for the introduction of a uniform and constant spatially averaged absorption coefficient of the gas as a surrogate for soot radiation. This approach has previously been used in the literature [18]. The value of the increased absorption coefficient due to the presence of soot is set by calibrating the model with experimental results. All surfaces are assumed to be black and the gas is assumed to be gray.

We model combustion with the laminar finite rate model, where reaction rates are determined by Arrhenius kinetic expressions [23]. This is appropriate given laminar/transitional nature of the flow. The source term for each species transport equation is given by the Arrhenius expression for each reaction involving that species in the chemical kinetic mechanism. We use the 11-species, 21-step skeletal reaction mechanism proposed by Hawkes et al. [24], a combined CO/H_2 combustion skeletal mechanism which was created by reducing a full chemical kinetic mechanism proposed by Li et al. [25] by analyzing data from laminar diffusion and premixed flames, homogeneous ignitions, and 2D unsteady jets. This mechanism is chosen because the predominant flammable components in the wood volatile composition considered (Table 1) are CO and H_2.

2.3. Boundary conditions

The model requires boundary conditions for the inlets, outlet, and stove walls. The air at the inlets is entrained by natural convection and thus we specify atmospheric pressure and temperature (300 K) and a turbulence intensity of 7.5%. The flow rate at the fuel inlet is specified as a mass flow rate with the flux of volatiles set by the desired burn rate of 2–5 kW, which is consistent with burn rates in cookstove modeling literature, as well as those observed in the lab and field [7,13,17]. The flux rate of volatiles entering the computational domain is set to match the desired burn rate. We do not model the conversion of solid fuel to volatiles, and the model does not provide a feedback mechanism from the flame to the fuel devolatilization process. A simplified composition of wood volatiles is taken from Galgano et al. [26] with minor modifications, shown in Table 1. The original composition contains ~6% CH_4, which we have converted to an equivalent amount of hydrogen on a heating value basis. This has a negligible effect on the heat release, but has the advantage of drastically reducing the size of the chemical kinetic mechanism since accurate modeling of CH_4 combustion requires roughly 50 species. The presence of tar has also been neglected.

The boundary condition at the outlet of the pot skirt is specified as atmospheric pressure. The cookpot is isothermal at the boiling point of water at atmospheric pressure (373 K). The combustion chamber, riser, cone deck, and pot skirt are modeled using a mixed convection,

Table 1
Mass fraction of species in wood volatile mix.

Species	CO	CO_2	H_2	H_2O
Mass Fraction	0.383	0.273	0.032	0.312

conduction, and radiation boundary condition. By this procedure, a heat transfer coefficient for each of the boundaries mentioned above is calculated. This combined heat transfer coefficient includes the effect of the wall thickness, insulation thickness and convection and radiation from the outer body to the environment. The external heat transfer coefficients are calculated using standard heat transfer correlations [27].

The simulations are carried out using the STAR-CCM + commercial software package using the finite volume method [28]. We use an unstructured polyhedral mesh selected after grid independence studies. Prism layers are added near the walls to adequately resolve the boundary layer in order to eliminate the need of wall functions in the turbulence model and accurately predict the heat transfer to the walls and the pot.

2.4. Model assumptions and limitations

In this work, we assume that the flow is statistically steady, and that an angular symmetry exists, such that the 3D geometry can be treated as an axisymmetric 2D geometry. We also assume a uniform absorption coefficient of gas inside the domain. Due to these assumptions, some non-axisymmetric geometric aspects of a side-fed stove are impossible to model accurately, such as the front entrance for the wood sticks and air, and the presence of a fuel grate. We do not consider the presence of the grate and use a simplified geometry upstream of the combustion chamber, which includes air entrainment from the primary air inlet at the bottom of the stove, and wood volatiles discharged uniformly from three toroidal fuel inlets. Due to the steady-state nature of the model, transient phenomena, such as the difference in flaming and char combustion at different times during the experiment and the changing water temperature, cannot be captured by the model. The advantage of the simplicity of the model is that it can be carried out with relatively modest computational resources (~2 hrs per simulation on a 16-core processor) and can accurately predict air flow characteristics and thermal efficiency as a function of stove geometry.

3. Experimental methods

We validate the computational model against a prototype wood stick side-fed, natural draft, rocket stove shown in Fig. 2. Engineering drawings of the stove are given in Section 1 of the supplement. The stove is 33 cm tall and 28 cm in diameter, with an 11 cm × 12 cm rectangular tunnel on one side for fueling. The feed tunnel extends towards the central vertical riser, which directs the hot combustion gases up towards the pot. The stove is equipped with a pot skirt, which keeps the hot gases in contact with the side of the pot. The stove is run on Douglas fir wood

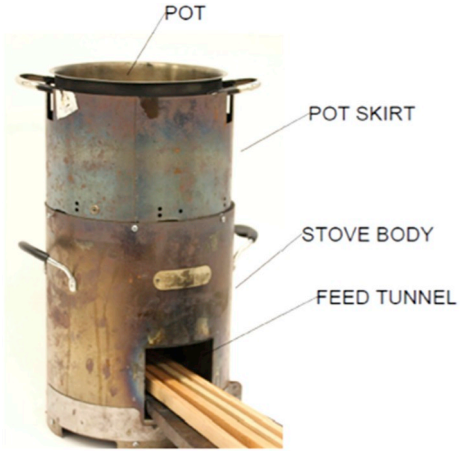

Fig. 2. Wood side fed, natural draft rocket stove used for experimental validation. The pot skirt sits on top of the stove body to keep the combustion gases in contact with the pot.

with a moisture content of 9.2%. The results of proximate and ultimate analyses of the wood performed according to the ASTM E870 standard are provided in Table 2. Wood sticks of approximate cross-section 20 mm × 20 mm are used. This is typically different from in-field use of biomass stoves, where biomass of several different sizes is burned.

3.1. Excess air measurement

We validate the model's prediction of the excess air that flows through the stove using experimental measurements of CO_2 exit concentrations. If we assume the fuel nitrogen content is negligible and that the fuel undergoes complete combustion (experiments show that the concentration of CO is less than 2% the concentration of CO_2), we can determine the excess air by rearranging the balanced combustion equation, to give us excess air as a function of the CO_2 concentration.

The balanced reaction equation for wood combustion, assuming that the nitrogen content of the wood is negligible is given as,

$$C_xH_yO_z + \varphi\left(x+\frac{y}{4}-\frac{z}{2}\right)(O_2+3.76N_2) \rightarrow xCO_2+\frac{y}{2}H_2O+3.76\varphi\left(x+\frac{y}{4}-\frac{z}{2}\right)N_2 + (\varphi-1)\left(x+\frac{y}{4}-\frac{z}{2}\right)O_2 \quad (2)$$

where x, y and z are kmoles of carbon, hydrogen and oxygen per 100 g of wood, calculated from the ultimate analysis of the fuel shown in Table 2. The measured CO_2 concentration y_{CO_2} can be written as the moles of CO_2 divided by the total moles of the products on the right hand side of the balanced reaction equation, which can then be rearranged to give us the air fuel ratio φ, or excess air,

$$Excess\ Air\ = (\varphi-1) = \left(\frac{\frac{x}{y_{CO_2}} - x - \frac{y}{2} + \left(x+\frac{y}{4}-\frac{z}{2}\right)}{4.76\left(x+\frac{y}{4}-\frac{z}{2}\right)} - 1\right) \quad (3)$$

During a test the stove is initially run on 4 sticks of wood as show in in Figure (3)A. Five liters of water is boiled from room temperature and then kept simmering within 5 °C of the local boiling temperature. We vary firepower between 1.5 kW and 5 kW during the simmer phase by controlling the amount of wood introduced into the cookstove. We use short tending intervals of 30 s–60 s to maintain a constant firepower. As a result, there is minimal char buildup and the dominant mode of heat release is flaming combustion. We use time averaged CO_2 concentration data during the simmer phase, where the measured CO_2 remains relatively constant, denoting constant firepower. The firepower is calculated by the mass rate of wood consumed multiplied by the heating value of the wood to give an energy produced per unit time.

Fig. 3(A) shows that the combustion gases are sampled from the top of the pot skirt in four representative locations (front, right side, left side, back) in an effort to obtain an average value. The gas is sampled using a four-pronged rake made from 4.76 mm OD stainless steel tubing. The stainless steel tubing is connected to 6.35 mm OD PVC tubing and converges into a single sample line. The flow is drawn by a bellows pump (MB-158, Senior Aerospace Metal Bellows, Sharon, MA), which feeds the sample flow to a CO_2 analyzer (PIR-2000, Horiba, Kyoto, Japan). The real-time mass of the cookstove is measured using a digital scale (ABK 70a, Adam Equipment, Danbury, CT).

Table 2
Proximate (dry basis) and ultimate analysis (dry, ash-free basis) of Douglas Fir wood.

Proximate Analysis (% mass)	Ash	Volatile Matter	Fixed Carbon		
	0.11	85.11	14.78		
Ultimate Analysis (% mass)	C	H	N	O	S
	50.62	5.92	0.09	43.21	0.05

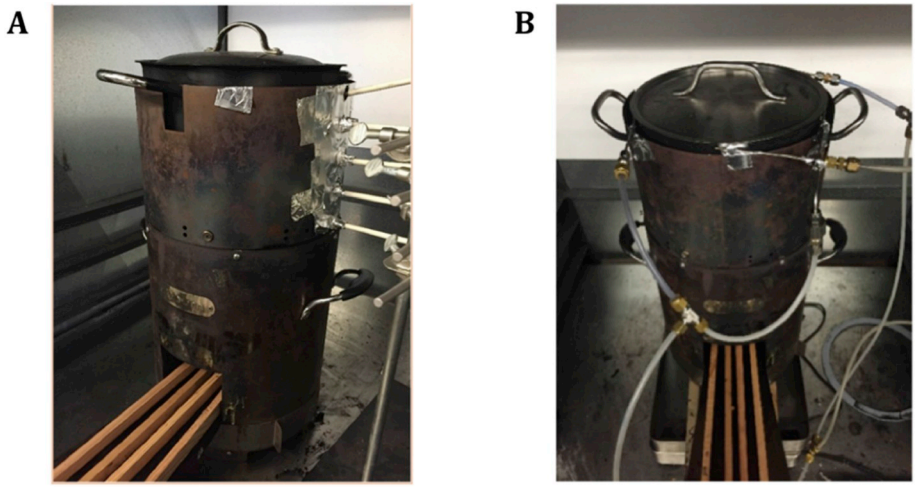

Fig. 3. (A) Experimental setup for measuring excess air within a natural draft cookstove. Four stainless steel probes sample the stove exhaust gases at the top of the pot skirt. These sample lines are combined into a single sample line that is routed to a CO_2 analyzer. (B) Experimental setup for measuring the temperature profile in the gap between the pot skirt and pot. Five K type thermocouples are used to measure the gas temperature at distances of 1.5, 5.5, 10, 14 and 17 cm from the bottom of the pot skirt.

3.2. Temperature measurements for model calibration

We measure gas temperatures in the gap between the pot and the pot skirt for calibrating the model to account for the presence of soot. We sample the gas at 1.5, 5.5, 10, 14, and 17 cm from the bottom of the pot skirt in a vertical line, as shown in Fig. 3(B). Type-K thermocouples (3859K44, McMaster-Carr, Elmhurst, IL) are used and thermally isolated from the skirt using fiberglass insulation wrapped around the probes (while keeping the junctions exposed) to prevent contact with the pot skirt. Tests are performed with the thermocouples located at the front, sides, and back of the cookstove, with the location varied by rotating the pot skirt and thermocouples. The tests are run in a very similar manner to the excess air tests, but with the firepower maintained as close to 4 kW as possible. The measured temperatures are averaged over short time periods where the average firepower is close to 4 kW.

Since we do not directly model soot, and thus do not know the values of the soot volume fraction, we instead account for the radiation heat transfer due to soot by employing an artificially high value of the gas absorption coefficient [18]. In this approach, the model is calibrated by adjusting the spatially uniform mean absorption coefficient (κ) in order to match experimentally measured temperature profiles in the cookstove as will be described in the results. The mean absorption coefficient for a luminous flame is given by $\kappa = 3.6\, cT_m/c_2$, where κ is the mean absorption coefficient in m^{-1}, T_m is the temperature in Kelvin, c_2 is the second constant of radiation, equal to $1.4388 \times 10^{-2}\, mK$ [30]. The constant C is defined as,

$$c = 36\pi f_v \frac{n^2 k}{\left[n^2 - (nk)^2 + 2\right]^2 + 4n^2k^2} \tag{4}$$

where n and k are the refractive and absorptive indices of refraction of the soot particles, respectively, and f_v is the soot volume fraction. Using values of n, k and f_v representative of hydrocarbon flames, Wohlgemuth et al. calculated the range of values the absorption coefficient can take to be between 0.03 m^{-1} and 11 m^{-1} [18]. The spatially averaged absorption coefficient should lie within this range of values. In real flames the absorption coefficient varies spatially and depends on the temperature and soot volume fraction.

4. Results and discussion

4.1. Calibration of absorption coefficient, κ

We first calibrate the spatially averaged absorption coefficient using average measured temperature data. Fig. 4 shows the gas temperature profile in the gap between the pot and the pot skirt as a function of height in the pot skirt ($z = 0$ is the bottom of the pot) (data shown are the average of the front, back, and side positions). The experimental data show that the temperature decreases with height in the riser as heat is transferred from the hot gases to the pot and the environment. The variation in measured temperatures around the circumference (shown by the error bars) is due to air from the inlet directing the flame towards the back of the riser, leading to a higher gas temperature in the back compared to the front; the CFD simulation is axisymmetric and does not capture this variation. We use the average measured temperature at each cross-section for the calibration procedure. We calibrate the model by varying the value of the gas absorption coefficient until the model temperature profile matches the experimental one, as shown in Fig. 4. An absorption coefficient of 7.5 m^{-1} is found to best match the experimental data. If we calculate the absorption coefficient only due to the presence of combustion gases, the temperature profile shown in Fig. 4 increases by approximately 200 K.

4.2. Relationship between firepower, airflow rate, and excess air

We use the model to examine the relationship between firepower and airflow rate. Fig. 5(A) shows a plot of the computed total, primary, and secondary air mass flow rates, as well as the experimentally measured total mass flow rate as a function of firepower. The total mass flow rate remains nearly constant with firepower, as observed in both measurement and computation. This is due to the competing effects of decreasing density and increasing volumetric flow rates due to increased gas temperatures. Increased fuel consumption results in higher gas temperatures

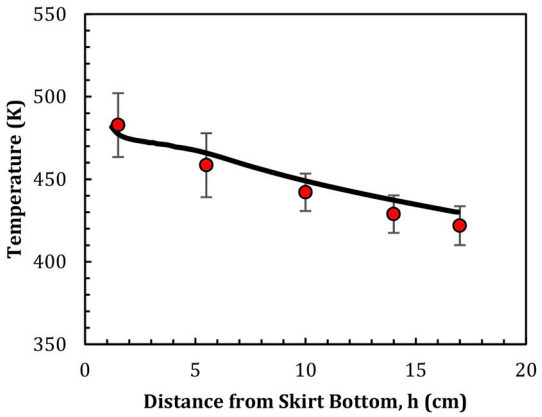

Fig. 4. Comparison of measured temperature profile (symbols) with calibrated temperature profile (line) in the gap between the pot and pot skirt.

inside the combustion chamber, which results in a greater buoyant force. The increased buoyant force leads to a greater velocity of the gas, and hence, an increased volumetric flow rate. However, the increased temperature also results in lower density, which leads to a relatively constant mass flow rate despite the increased volumetric flow rate over a wide range of firepowers. This effect of having a relatively constant mass flow rate over this range of firepowers is also observed in the predictions made by Agenbroad et al. [13], for which they provide a similar reasoning. From the figure, we also observe that the primary and secondary air flow rates stay fairly constant with increasing firepower. Fig. 5(B) shows a plot of the excess air through the stove as a function of firepower for the CFD model and experiments. A constant air mass flow rate results in a lower excess air with increasing firepower, since more fuel is being injected with no change in airflow. At a low firepower of 2 kW, the amount of air present in the system is in excess of ten times what is required for complete combustion. At the highest fire power examined (5 kW), the excess air is still more than three times greater than what is required. Some excess air is recommended to enhance mixing and avoid rich combustion that could result in unwanted soot production [31]. Conversely, too much cool air flowing through the stove cools the combustion gases and can diminish heat transfer to the pot and degrade the thermal efficiency, as was also hypothesized by Baldwin [12].

4.3. Effect of baffles and secondary air entrainment

A method of reducing the excess air in a cookstove is the placement of a central baffle in the riser. The baffle will (1) reduce air flow via introducing an additional pressure drop, and (2) potentially enhance mixing by creating a more complex flow field. We examine the effect of baffle size on the airflow rate, thermal efficiency and mixing. The OH mass fraction, temperature distribution and the turbulent kinetic energy inside a cookstove with secondary air and with and without a central baffle are shown in Fig. 6. Fig. 6(A) and (B) show the computed OH mass fraction and temperature distribution inside the cookstove with secondary air injection. The OH radical is highly reactive and short-lived, and hence can be used to track the position of the flame front [23]. The flame is a diffusion flame and can be seen as a thin sheet of high OH concentration that sits at the intersection of the air and fuel in Fig. 6(A). Note that the flame front denoted by high OH concentration is also the hottest part of the flame. Fig. 6(B) shows the temperature distribution in the stove which varies from 1800 K in the flame front to 300 K at the air inlet. A zone of cold air is seen around the flame, which does not contribute to the combustion, but mixes with the burned gases further downstream and reduces the bulk gas temperature, which leads to a reduction in heat transfer to the pot. The cold air entering from the secondary air inlet does not penetrate the main flow and moves up along the riser wall. The turbulent kinetic energy distribution with secondary air, shown in Fig. 6(C) shows very little turbulence in the region within the flame sheet. This is evidence that in this case the secondary air does not significantly contribute to mixing inside the stove.

Fig. 6(D), (E) and (F) show the OH mass fraction, temperature distribution, and turbulent kinetic energy distribution inside the cookstove with secondary air and a central baffle blocking 45% of the riser area. When we add the baffle to the stove the temperature distribution is more uniform in the region above the riser and the turbulent kinetic energy is greater, suggesting enhanced mixing in the upper part of the riser. The presence of the baffle causes the flame to break up, as seen in the temperature distribution and OH mass fraction plots. The presence of the baffle also results in a reduction in the primary airflow rate, from 0.0034 kg s^{-1} to 0.0025 kg s^{-1} due to the flow obstruction caused by the baffle. The secondary airflow rate remains approximately the same when the baffle is present. Together, the baffle and secondary air flow results in better mixing downstream of the baffle, as is seen from the more uniform temperature distribution and greater turbulent energy. Higher temperatures and increased turbulent mixing have been linked to lower PM emissions in cookstoves [32].

Fig. 7(A) shows plots of primary, secondary and total air mass flow rates as a function of the percentage of riser area blocked by the central baffle, at a constant firepower of 4 kW. When no baffle is present, the airflow rate is nearly evenly divided between the primary and secondary air. The primary air flow rate decreases with increasing baffle size, since the baffle obstructs the primary air. At 75% riser area blockage, only 25% of the total airflow is contributed by the primary air. Fig. 7(B) shows the effect of increasing baffle size on the stove efficiency. The stove efficiency reduces slightly as the baffle size is increased. When flow is blocked by a central baffle, the reduced airflow rate leads to higher bulk temperatures, and more heat is absorbed by the riser walls and cone deck due to better mixing. Therefore, despite a reduction in the airflow rate, thermal efficiency is reduced.

4.4. Effect of cone-deck shape and pot support height

Next, we examine the effect of the shape of the cone deck on the thermal efficiency and airflow rate. The cone deck is the part of the cookstove placed on top of the riser. It serves as a gradual area expansion for the gas flow, which mitigates the effects of flow separation and directs flow under the bottom of the pot. A sample cone deck and its placement on a cookstove is shown in Fig. 8(a) and (b).

An often quoted rule-of-thumb states that for optimal heat transfer to the pot, the cross-sectional area of the flow path throughout the cookstove should be constant, including the flow area over the cone deck [33,34]. To examine the robustness of this guideline, we present results on how the shape of the cone deck influences performance parameters such as thermal efficiency and airflow rate. We define the cone deck using three geometric parameters, as shown in Fig. 9: the horizontal distance from the centerline to the far end of the slanted region, X, the vertical distance between the top and bottom of the slanted region, Y, and the height of the pot supports. A total of 36 cone decks are modeled, with X values of 79 mm, 108 mm, 138 mm and 168 mm, Y values of 8 mm,

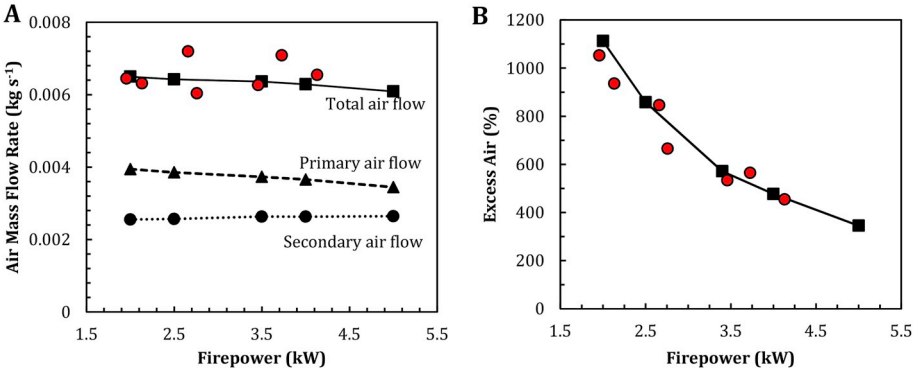

Fig. 5. (A) Plot of airflow rate as a function of firepower. The circular red markers are experimental results. The square, triangular, and circular black markers are the total, primary and secondary air mass flow rates predicted by the CFD model, respectively. (B) Plot of excess air as a function of firepower of cookstove. The circular markers are experimental results and the square markers are results obtained from the CFD model. (For interpretation of the references to colour in this figure legend, the reader is referred to the Web version of this article.)

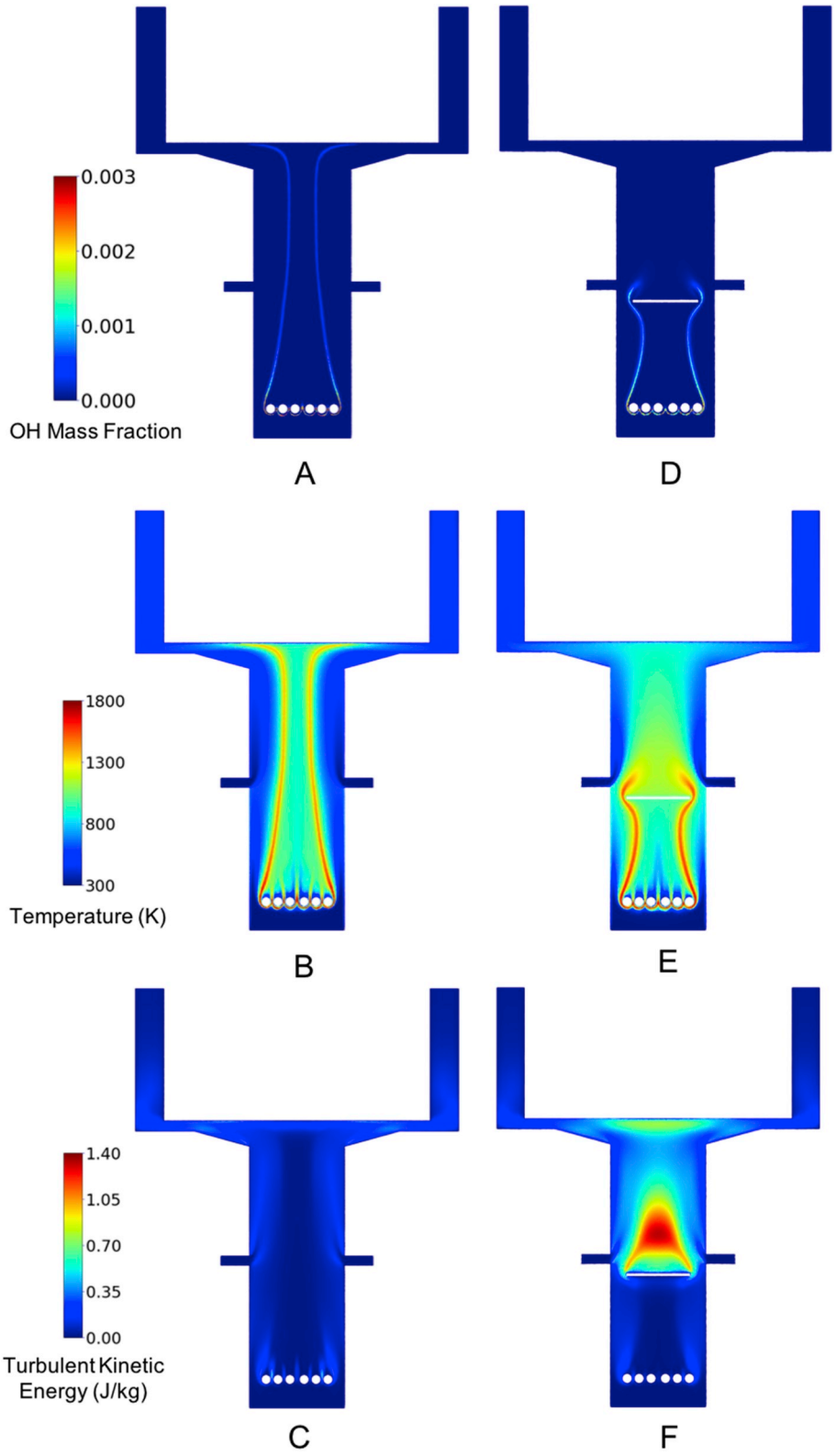

Fig. 6. (A) Computed OH mass fraction with secondary air. (B) Computed OH mass fraction with secondary air and central baffle blocking 45% of riser area. (C) Computed temperature distribution with secondary air. (D) Computed temperature distribution with secondary air and central baffle blocking 45% of riser area. (E) Computed turbulent kinetic energy with secondary air. (F) Computed turbulent kinetic energy with secondary air and central baffle blocking 45% of riser area.

16 mm, and 24 mm and pot support height values of 7 mm, 9 mm, and 11 mm. Each possible combination of *X*, *Y* and the pot support height is modeled for a constant firepower of 4 kW.

Fig. 10 shows a subset of the results of this study. Fig. 10(a) shows the thermal efficiency as a function of X while Fig. 11(b) shows the thermal efficiency as a function of pot support height. Each curve represents a constant Y. The thermal efficiency reduces as X increases, and for a constant X, reduces as Y increases. The difference in efficiency between a

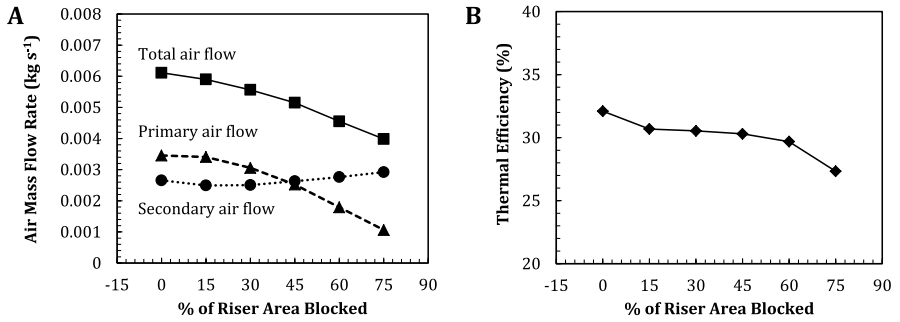

Fig. 7. (A) Primary (dashed line, triangular), secondary (dotted line, circular), and total (solid line, square) airflow rate as a function of riser area blocked by central baffle predicted by the model. The total airflow reduces as the size of the baffle is increased. The contribution of primary air reduces, and that of secondary air increases with increasing baffle size. (B) Stove efficiency predicted by the model as a function of riser area blocked by central baffle. The efficiency decreases slightly as baffle size increases.

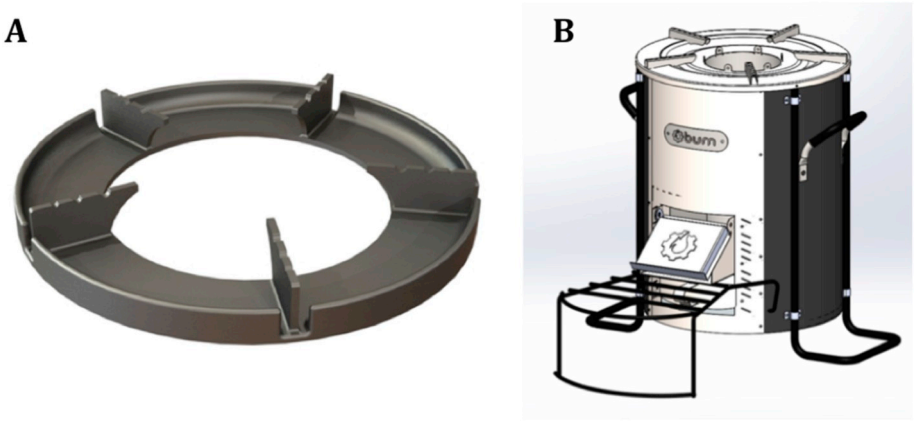

Fig. 8. (a) Example of a cone deck. (b) Position of cone deck on a cookstove (courtesy of Burn Design Lab.).

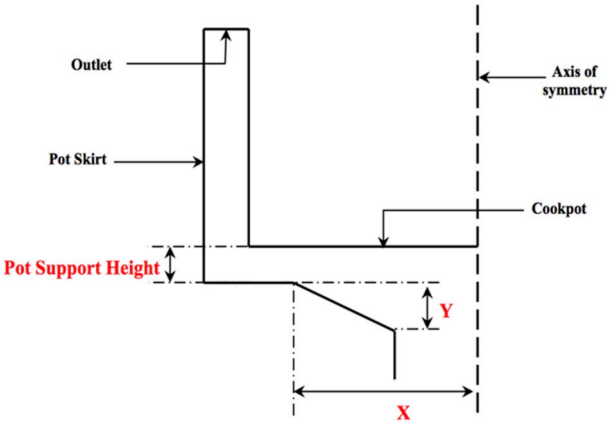

Fig. 9. Geometric parameters defining cone deck shape.

Y of 8 mm and 16 mm is much greater than the difference between a Y of 16 mm and 24 mm, provided that the firepower can be held relatively constant. Therefore, the plot suggests that a 'flatter' cone deck (low Y) is better than a 'steeper' design (high Y). From Fig. 10(b), we observe that reducing the pot support height increases the thermal efficiency irrespective of Y. This corresponds to a reduction in airflow rate (shown in Section 4 of the supplement).

Based on this analysis (complete results shown in Section 4 of the supplement), three cone deck configurations were fabricated and tested. The configurations are as follows:

- Configuration 1: X = 108 mm, Y = 20 mm, Pot support height = 11 mm
- Configuration 2: X = 108 mm, Y = 10 mm, Pot support height = 11 mm
- Configuration 3: X = 108 mm, Y = 10 mm, Pot support height = 9 mm

Configuration 1 is the baseline configuration before the study was conducted. The X value is not changed since it is fixed by the manufacturing process. For Configuration 2, the Y value is dropped, since an increase in thermal efficiency was expected. In Configuration 3, the pot support height is dropped to 9 mm in order to further increase thermal efficiency. The cone decks were tested at an average firepower of 3.5 kW. Fig. 11 shows the comparison of the results of experiments and numerical simulations for each configuration. The model's predictions of thermal efficiency for each configuration is close to the experimental results and shows the same trends. The model underpredicts the experimentally measured efficiency by 1.78% on average. We hypothesize that this is due to variation in experimental quantities that are held constant in the simulation, such as firepower. Configuration 3 gives the best performance, with an average thermal efficiency of 35.9%, an increase of 6.8% over Configuration 1 and 5.5% over Configuration 2.

In order to understand the effect of the shape of the cone deck on the thermal efficiency, we plot the thermal efficiency of the cookstove as a function of the airflow rate through the cookstove, shown in Fig. 12(a). We observe that the efficiency of the cookstove, for differing cone deck configurations, is linearly dependent on the air flow rate through the cookstove. These data suggest that the shape of the cone deck controls the flow of air through the cookstove via the different pressure drops associated with the designs. We hypothesize that the increased pressure drop due to more constricted designs leads to an increase in the bulk temperature of the gas, which in turn increases heat transfer to the cookpot and efficiency. Fig. 12(b) shows that the averaged gas temperature at the riser outlet increases with reduced air mass flow rate,

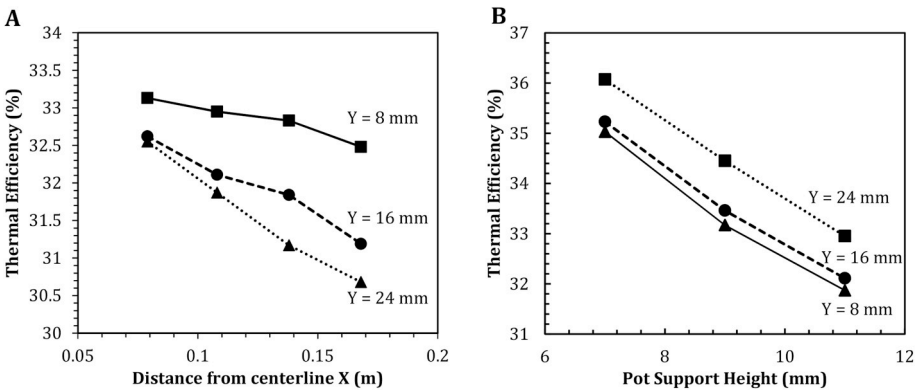

Fig. 10. (a) Thermal efficiency as a function of X for a pot support height of 11 mm. The solid curve is for a Y of 8 mm, the dashed curve is for a Y of 16 mm, and the dotted curve is for a Y of 24 mm. (b) Thermal efficiency as a function of pot support height for a constant X of 108 mm. Each curve represents the same Y as (a). All curves are for a constant firepower of 4 kW.

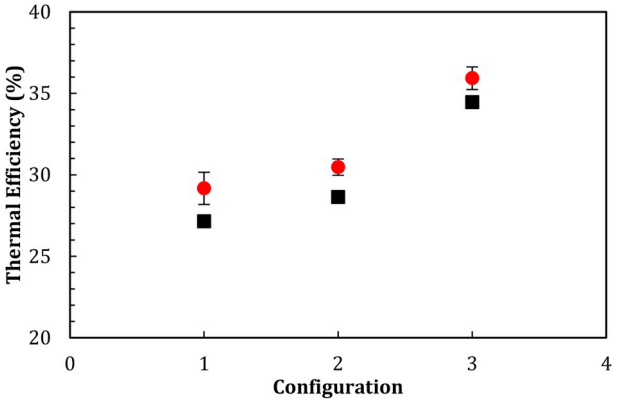

Fig. 11. Thermal efficiency of three cone deck configurations. The red markers are experimental results with 90% confidence intervals and the black markers are numerical results. Configuration 1 is a cone deck with X = 108 mm, Y = 20 mm, and pot support height = 11 mm. Configuration 2 is a cone deck with X = 108 mm, Y = 10 mm and pot support height = 11 mm. Configuration 3 is a cone deck with X = 108 mm, Y = 10 mm and pot support height = 9 mm. (For interpretation of the references to colour in this figure legend, the reader is referred to the Web version of this article.)

which supports the hypothesis that pressure drop and total air flow rate impact efficiency through the average gas temperature.

4.5. Relationship between airflow rate and thermal efficiency

We further examine the relationship between airflow rate and efficiency by comparing the pressure drop across the cookstove for different baffle and cone deck configurations. Fig. 13(a) shows the predicted mass flow rates through the cookstove as a function of the predicted pressure drop through the cookstove for various baffle and cone deck configurations. The mass flow rate through the stove is inversely related to the pressure drop, as expected. The thermal efficiency as a function of the pressure drop in Fig. 13(b) shows two distinct behaviors. In the variations of cone deck configurations, the thermal efficiency increases linearly with the pressure drop suggesting that the decrease in air flow results in higher efficiency due an increase in average bulk temperature. In the case of the baffles, the increasing pressure drop was associated with a decrease in thermal efficiency because the of the loss of heat to the walls due to enhanced mixing. This supports the hypothesis that only reducing excess air might not lead to an increase in thermal efficiency; the location where flow is obstructed is important, and needs careful consideration.

5. Conclusion

This paper examines the performance of a wood burning, natural draft rocket cookstove through numerical simulation and experiment. The relationships between firepower, airflow rate, excess air, and thermal efficiency are explored, and the effect of various geometric features on these quantities is analyzed.

It is found that wood-burning natural draft rocket cookstoves operate at excess air percentages several times stoichiometric air for almost every configuration studied, except where the flow is severely constricted due to a narrow passage. Despite an abundant quantity of air present in the cookstove, little mixing is observed in most configurations, even with secondary air entrainment. The exception is when a

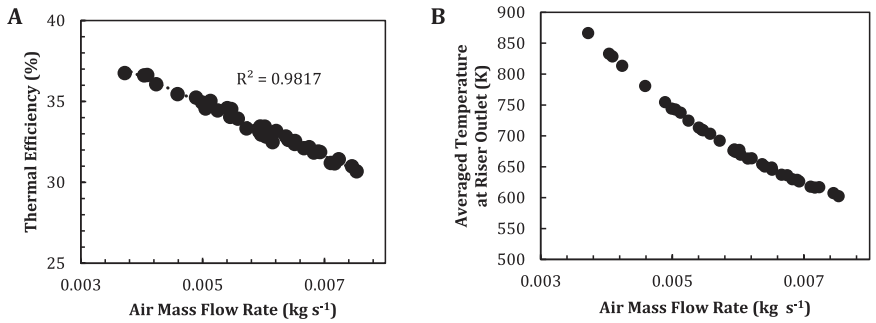

Fig. 12. Predicted thermal efficiencies and bulk temperatures for various cone decks configurations (a) Thermal efficiency as a function of air mass flow rate. Each point represents a specific cone deck configuration. The dotted line is a linear trend line. (b) Mass-averaged temperature at the mouth of the riser as a function of air mass flow rate. Each point represents a specific cone deck configuration.

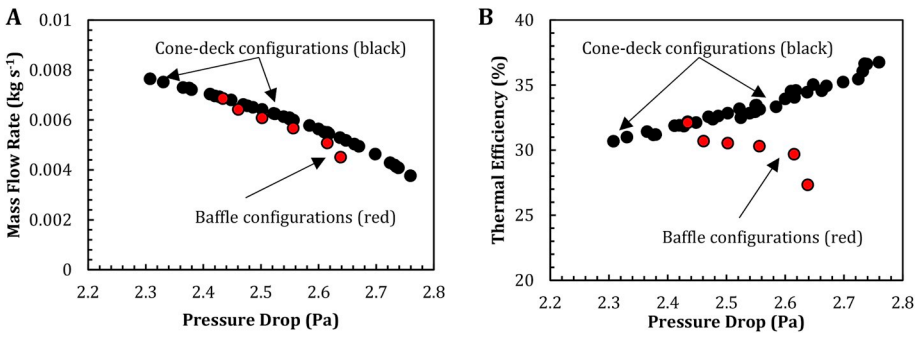

Fig. 13. Predicted mass flow rates and thermal efficiencies for various cone deck configurations and baffle sizes. Each point represents a specific cone deck/baffle configuration. Black markers represent cone deck configurations and red markers represent baffle configurations. (a) Mass flow rate through the cookstove as a function of predicted pressure drop. (b) Thermal efficiency of cookstove as a function of predicted pressure drop. (For interpretation of the references to colour in this figure legend, the reader is referred to the Web version of this article.)

central baffle is introduced into the riser, which increases the turbulent mixing downstream of the obstruction.

The excess air is observed to be an important factor in controlling the thermal efficiency of the rocket cookstove for the configurations investigated. Two geometric features of the cookstove, the pot support height and the cone deck shape are found to control the airflow rate through the cookstove, with more restrictive designs reducing the excess air and promoting heat transfer to the cookpot. This contradicts a prevalent design guideline which states that the cross-sectional area of the flow path through the cookstove should be constant for optimal heat transfer to the pot.

Counterintuitively, the introduction of a central baffle, a geometric feature often used specifically to reduce the airflow rate, leads to a reduction in the thermal efficiency of the cookstove despite decreased excess air flow. This is found to be due to increased heat loss to the walls of the cookstove, which is a result of the increased turbulent mixing downstream of the baffle. This suggests that care should be taken when reducing excess air flow in the stove to avoid increasing heat transfer to the stove body or the environment.

Acknowledgments

This research was sponsored by the US Department of Energy under the DOE BETO Cookstoves Program grant number DE -EE0006284 with Elliott Levine as program manager. Computations were performed on the Hyak supercomputer system at the University of Washington.

Appendix A. Supplementary data

Supplementary data to this article can be found online at https://doi.org/10.1016/j.biombioe.2019.105402.

References

[1] S. Bonjour, H. Adair-Rohani, J. Wolf, N.G. Bruce, S. Mehta, A. Prüss-Ustün, M. Lahiff, E.A. Rehfuess, V. Mishra, K.R. Smith, Solid fuel use for household cooking: country and regional estimates for 1980–2010, Environ. Health Perspect. 121 (7) (2013) 784–790.
[2] P.H.N. Saldiva, S.G.E.K. Miraglia, Health effects of cookstove emissions, Energy Sustain. Dev. 8 (3) (2004) 13–19.
[3] N. Bruce, D. Pope, E. Rehfuess, K. Balakrishnan, H. Adair-Rohani, C. Dora, "WHO indoor air quality guidelines on household fuel combustion: strategy implications of new evidence on interventions and exposure–risk functions, Atmos. Environ. 106 (2015) 451–457.
[4] V. Ramanathan, G. Carmichael, Global and regional climate changes due to black carbon, Nat. Geosci. 1 (4) (2008) 221–227.
[5] M. Tucker, Can solar cooking save the forests? Ecol. Econ. 31 (1) (1999) 77–89.
[6] Water boiling test protocol, Version 4.2.3" [Online]. Available: http://cleancookstoves.org/technology-and-fuels/testing/protocols.html.
[7] J. Jetter, Y. Zhao, K.R. Smith, B. Khan, T. Yelverton, P. DeCarlo, M.D. Hays, Pollutant emissions and energy efficiency under controlled conditions for household biomass cookstoves and implications for metrics useful in setting international test standards, Environ. Sci. Technol. 46 (19) (2012) 10827–10834.
[8] C.A. Roden, T.C. Bond, S. Conway, A.B. Osorto Pinel, N. MacCarty, D. Still, Laboratory and field investigations of particulate and carbon monoxide emissions from traditional and improved cookstoves, Atmos. Environ. 43 (6) (2009) 1170–1181.
[9] K.R. Smith, K. Dutta, C. Chengappa, P.P.S. Gusain, O. Masera, V. Berrueta, R. Edwards, R. Bailis, K.N. Shields, Monitoring and evaluation of improved biomass cookstove programs for indoor air quality and stove performance: conclusions from the household energy and health project, Energy Sustain. Dev. 11 (2) (2007) 5–18.
[10] M.P. Kshirsagar, V.R. Kalamkar, A comprehensive review on biomass cookstoves and a systematic approach for modern cookstove design, Renew. Sustain. Energy Rev. 30 (2014) 580–603.
[11] N.A. MacCarty, K.M. Bryden, Modeling of household biomass cookstoves: a review, Energy Sustain. Dev. 26 (2015) 1–13.
[12] S.F. Baldwin, *Biomass Stoves: Engineering Design, Development, and Dissemination*, Volunteers in Technical Assistance ; Center for Energy and Environmental Studies, Princeton University, Arlington, Va., USA : Princeton, N.J., USA, 1987.
[13] J. Agenbroad, M. DeFoort, A. Kirkpatrick, C. Kreutzer, "A simplified model for understanding natural convection driven biomass cooking stoves—Part 1: setup and baseline validation, Energy Sustain. Dev. 15 (2) (2011) 160–168.
[14] J. Agenbroad, M. DeFoort, A. Kirkpatrick, C. Kreutzer, "A simplified model for understanding natural convection driven biomass cooking stoves—Part 2: with cook piece operation and the dimensionless form, Energy Sustain. Dev. 15 (2) (2011) 169–175.
[15] R. Shah, A.W. Date, Steady-state thermochemical model of a wood-burning cookstove, Combust. Sci. Technol. 183 (4) (2011) 321–346.
[16] H. Burnham-Slipper, Breeding a Better Stove: the Use of Computational Fluid Dynamics and Genetic Algorithms to Optimise a Wood Burning Stove for Eritrea, University of Nottingham, 2009.
[17] D.D. Miller-Lionberg, A Fine Resolution CFD Simulation Approach for Biomass Cook Stove Development, Colorado State University, 2011.
[18] A. Wohlgemuth, S. Mazumder, D. Andreatta, Computational heat transfer analysis of the effect of skirts on the performance of third-world cookstoves, J. Therm. Sci. Eng. Appl. 1 (4) (2009), 041001.
[19] K.M. Bryden, D.A. Ashlock, D.S. McCorkle, G.L. Urban, Optimization of heat transfer utilizing graph based evolutionary algorithms, Int. J. Heat Fluid Flow 24 (2) (2003) 267–277.
[20] T.-H. Shih, W.W. Liou, A. Shabbir, Z. Yang, J. Zhu, "A new K-ε eddy viscosity model for high Reynolds number turbulent flows," comput, Fluid 24 (3) (1995) 227–238.
[21] S. Pope, Turbulent Flows, Cambridge University Press, New York, 2001.
[22] M. Modest, Radiative Heat Transfer, Academic Press, 2003.
[23] I. Glassman, R.A. Yetter, Combustion, Academic Press, 2008.
[24] E.R. Hawkes, R. Sankaran, J.C. Sutherland, J.H. Chen, Scalar mixing in direct numerical simulations of temporally evolving plane jet flames with skeletal CO/H2 kinetics, Proc. Combust. Inst. 31 (1) (2007) 1633–1640.
[25] J. Li, Z. Zhao, A. Kazakov, M. Chaos, F.L. Dryer, J.J. Scire, A comprehensive kinetic mechanism for CO, CH2O, and CH3OH combustion, Int. J. Chem. Kinet. 39 (3) (2007) 109–136.
[26] A. Galgano, C. di Blasi, Coupling a CFD code with a solid-phase combustion model, Prog. Comput. Fluid Dyn. 6 (4–5) (2006) 287–302.
[27] F.P. Incropera, D.P. DeWitt, Fundamentals and Heat and Mass Transfer, John Wiley and Sons, 2002.
[28] STAR CCM+ user manual, CD-Adapco [Online]. Available: https://thesteveportal.plm.automation.siemens.com.
[30] W.W. Yuen, C.L. Tien, A simple calculation scheme for the luminous-flame emissivity, in: Symposium (International) on Combustion, Elsevier, 1977, pp. 1481–1487.
[31] K.B. Sutar, S. Kohli, M.R. Ravi, A. Ray, Biomass cookstoves: a review of technical aspects, Renew. Sustain. Energy Rev. 41 (2015) 1128–1166.
[32] V.H. Rapp, J.J. Caubel, D.L. Wilson, A.J. Gadgil, Reducing ultrafine particle emissions using air injection in wood-burning cookstoves, Environ. Sci. Technol. 50 (15) (2016) 8368–8374.
[33] Dean Still, Jim Kness, Aprovecho Research Center, Capturing Heat : Five Earth-Friendly Cooking Technologies and How to Build Them, Aprovecho Research Center, Cottage Grove, 1996. OR (80574 Hazelton Rd., Cottage Grove, OR 97424).
[34] Bryden, K. M., Still, D., Scott, P., Hoffa, G., Ogle, D., Balis, R., and Goyer, K., Design Principles for Wood Burning Cookstoves, Aprovecho Research Center.